Received: 31 July 2019 | Revised: 7 May 2020 | Accepted: 8 May 2020

DOI: 10.1002/stc.2575

WILEY

RESEARCH ARTICLE

Bayesian dynamic forecasting of structural strain response using structural health monitoring data

Y.W. Wang[1,2] | **Y.Q. Ni**[1,2]

[1]Department of Civil and Environmental Engineering, The Hong Kong Polytechnic University, Kowloon, Hong Kong

[2]National Rail Transit Electrification and Automation Engineering Technology Research Center (Hong Kong Branch), The Hong Kong Polytechnic University, Kowloon, Hong Kong

Correspondence
Y.Q. Ni, Department of Civil and Environmental Engineering, The Hong Kong Polytechnic University, Hung Hom, Kowloon, Hong Kong.
Email: ceyqni@polyu.edu.hk

Funding information
Innovation and Technology Commission of Hong Kong SAR Government, Grant/Award Number: K-BBY1; National Natural Science Foundation of China, Grant/Award Number: U1934209; Research Grants Council of the Hong Kong Special Administrative Region (SAR), China, Grant/Award Number: PolyU 152024/17E

Summary

Research on structural health monitoring (SHM) is nowadays evolving from SHM-based diagnosis towards SHM-based prognosis. The structural strain response, as a localized response, has gained growing attention for application to structural condition assessment and prognosis in that continuous strain measurement can offer information about the stress experienced by an in-service structure and is better suited to characterize local deficiency and damage of the structure than global responses. As such, accurate forecasting of the structural strain response in real time is essential for both structural condition diagnosis and prognosis. In this paper, a Bayesian modeling approach embedding model class selection is proposed for dynamic forecasting purpose, which enables the probabilistic forecasting of structural strain response and bears a strong capability of modeling the underlying non-stationary dynamic process. As opposed to the classical time series models, the proposed Bayesian dynamic linear model (BDLM) accommodates both stationary and non-stationary time series data and delineates the time-dependent structural strain response through invoking different hidden components, such as overall trend, seasonal (cyclical), and regressive components. It in turn paves an effective way for incorporating the newly observed time-variant data into the model framework for structural response prediction. By embedding a novel model class selection paradigm into the BDLM, the proposed algorithm enables simultaneous model class selection and probabilistic forecasting of strain responses in a real-time manner. The utility of the proposed approach and its forecasting accuracy are examined by using the real-world monitoring data successively collected from a three-tower cable-stayed bridge.

KEYWORDS

Bayesian model class selection, Bayesian dynamic linear model, real-time structural condition prediction, strain response, structural health monitoring

1 | INTRODUCTION

Critical civil infrastructures such as large dams, long-span bridges, supertall buildings, and high-speed railways, among many others, are significant pillars of modern civilization. These structures will gradually deteriorate or disintegrate as they are constantly subjected to operational loadings and environmental attacks and sometimes to extreme events such as earthquakes, tornadoes, and typhoons. Deficiency in these vital infrastructures could pose major threats to public safety and even devastate the society and economy. Structural health monitoring (SHM) is well recognized as a viable technology helping to secure the structural and operational safety of infrastructure systems and issue an early warning of damage in time to prevent costly repairs or even catastrophic failure. The SHM systems provide an insight into the "fitness for purpose" of structures undergoing gradual or sudden changes in condition and also of the loadings actually acting on the structures and the response mechanisms.[1] The past two decades have witnessed a rapid increase in multidisciplinary research on SHM and its applications to a wide variety of infrastructures.[2–5] Over the past decades, many scholars have been engaged in developing vibration-based structural damage detection/diagnosis methods in either deterministic or probabilistic context.[6–17]

Although the vibration-based methods using acceleration data have been successfully applied for structural health diagnosis and damage detection, a methodological framework suitable for interpreting strain data in time series is more favorable for structural health prognosis. The real-time monitoring data of structural strain response during in-service operation are particularly meaningful in that (i) continuous strain measurement can offer information about the stress experienced by the structure under in-service conditions, and (ii) strains are better suited to characterize the local deficiency and damage of a structure than globalresponses.[18] A rational prediction of time-varying structural strain behavior using SHM-based strain data poses certain challenges.[19] Its practical application in forecasting strain response is inevitably hindered by the non-stationary feature and uncertainty inherent in the monitoring data.

In the SHM community, forecasting techniques have been widely investigated and reported in the literature, such as statistical models,[20] time series models,[21,22] support vector machine,[23] and singular spectrum analysis (SSA) technique.[24,25] As a kind of process-specific Bayesian prediction model, the Bayesian dynamic linear model (BDLM) has been increasingly viewed as a highly promising modeling technique in the fields of statistics and economics,[26,27] especially after the advent of Markov chain Monte Carlo (MCMC) algorithms. However, Bayesian time series analysis using BDLM has not been much explored in the field of civil engineering. Solhjell[28] made the first attempt to deploy BDLM in connection with SHM. Recently, Goulet and his coworker[29,30] addressed SHM-relevant issues in the context of BDLM, where they modeled the time-dependent response of a structure by decomposing it into subcomponents, with the model parameters estimated utilizing an expectation maximization (EM) algorithm. The increasing applications of BDLM indifferent fields can be attributed to three admirable merits. First, in contrast to classical autoregressive and moving average (ARMA) models that rest on stationarity, the BDLM accommodates both stationary and non-stationary time series data with time-varying model coefficients. Second, the BDLM can incorporate newly acquired observations to update the model and provide ahead forecasts without the need of reconstructing the BDLM. Third, the BDLM provides a perfect tool for characterizing the uncertainty in time series and quantifying the uncertainty of forecasts. These three noteworthy features render the BDLM approach favorably suitable for forecasting the strain response of an in-service structure using SHM data. The first feature guarantees the ability to characterize non-stationary strain response, the second makes for convenient and efficient forecasts, and the third allows for an assessment of the degree of uncertainty in structural strain forecasts. In addition to the above features, the ability of BDLM enabling the prediction of conditional probabilities can be utilized for real-time damage detection. Once the BDLM is available, one-step (or multistep) forecasting probability density function (PDF) can be obtained before proceeding to the next observation. This prediction model and its alternative model (which is usually formulated by shifting the mean value by a prescribed offset) can be statistically compared to determine which better fits the actual observation. If the comparison results are in favor of the alternative model, it is claimed that a potential change has occurred. Then the Bayes factor and cumulative Bayes factor in line with Bayesian hypothesis testing can be elicited to accomplish outlier identification and damage detection.[31]

Although the structural response prediction with a prescribed BDLM using SHM data is achievable without much difficulty, the problem of model class selection in a real-time manner remains a challenge and has seldom been studied. With a set of model class candidates (e.g., assorted candidate BDLMs representing the different combinations of trend, seasonal [cyclical] and regression effects), it is obvious that a more complicated model, with more adjustable parameters, often better fits the observations than a simple model with fewer parameters. The sole consideration of data fitting quality, however, leads to unnecessarily complicated model class that gives poor predictions and most likely, overfitting.

In view of this, the selected model class should strike a balance between the forecast performance and parameter complexity. The majority of the studies on Bayesian model class selection (BMCS) were conducted in an offline manner,[9,32–34] except for a recent work on real-time system identification.[16]

In this article, a novel Bayesian real-time algorithm embedding model class selection is proposed for probabilistic forecasting of time-dependent structural strain response given SHM data. The innovative contributions of this paper are that, in order to appropriately determine the response components (trend, seasonal/cyclical, and regression components) and their combinations, BMCS is embedded into the modeling process of BDLM by which the optimal model with most appropriate components and their order is elicited to characterize the time series of strain response, thus enabling concurrently model class selection and probabilistic forecasts in a real-time manner. To achieve this, a Gibbs sampling algorithm is utilized to simultaneously infer the latent states, the parameters of state dynamics, and the marginal likelihood for model selection. The rest of the paper is organized as follows. Section 2 presents the general formulation of BDLM and the model components. In Section 3, a general procedure is elaborated for applying the Gibbs sampler technique to model parameters estimation and structural response forecasting. A real-time model class selection method in line with BDLM is described in Section 4. In Section 5, the proposed method for non-stationary time-dependent structural strain response forecasting is validated using the real-world monitoring data collected from the cable-stayed Ting Kau Bridge (TKB). Conclusions are drawn in Section 6.

2 | REAL-TIME FORECAST WITH BDLM

2.1 | Bayesian dynamic linear model

The physical parameters descriptive of a dynamic system, in general, vary continuously over time and are observed (monitored) at discrete time instants, $t = 1,...,T$. In this study, a DLM is used to underpin the methodological framework for estimation and prognosis of structural condition/health with the direct use of strain monitoring data in time domain. The DLM is much simpler than the general state-space model yet provides flexibility. In general, the DLM can be expressed to comprise an observation (measurement) equation and a system (transition) equation as follows[26]:

$$\text{Observation equation}: y_t = F_t'\theta_t + v_t\, v_t\tilde{N}[0, V_t], \tag{1}$$

$$\text{System equation}: \theta_t = G_t\theta_{t-1} + \omega_t\, \omega_t\tilde{N}[0, W_t], \tag{2}$$

where y_t is the observation (measurement) vector of $(m \times 1)$ at time t; θ_t is an unknown state parameter vector of $(p \times 1)$; F_t and G_t are known regression matrix of $(p \times m)$ and evolution matrix of $(p \times p)$, respectively; v_t and ω_t are two independent Gaussian random vectors with zero mean and unknown covariance matrices V_t and W_t, respectively. The DLM defined above amounts to treating θ_t as a Markov chain and y_t being independent conditionally on θ_t; that is, $\theta_t \mid \theta_{t-1} \sim N(G_t\theta_{t-1}, W_t)$ and $y_t \mid \theta_t \tilde{N}\left(F_t'\theta_t, V_t\right)$.

In a Bayesian setting, the DLM provides a probabilistic linkage to update the posterior distribution of state parameters based on a prior distribution and newly available observation over time. The details of using DLM for recursive one-step ahead forecasting under Bayesian framework were given in Solhjell.[28] Assume that the posterior distribution of state parameters $P(\theta_t \mid D_t)$ is known at time t and conforms to a normal distribution $P(\theta_t \mid D_t) \sim N(m_t, C_t)$, given the observed time series data $\{y_1, y_2, ..., y_t\}$ and other related information. The prior distribution of the state parameters $P(\theta_{t+1} \mid D_t) \sim N(a_{t+1}, R_{t+1})$ at next time $t+1$ can be obtained from the system equation (Equation 2) as

$$a_{t+1} = E[\theta_{t+1}|D_t] = G_{t+1}m_t; R_{t+1} = Var[\theta_{t+1}|D_t] = G_{t+1}C_tG_{t+1}' + W_t, \tag{3}$$

where $D_t = \{D_{t-1}, y_t\}$ denotes the information at time t, which is determined recursively given the initial prior information D_0 at $t = 0$; W_{t+1} represents the extrauncertainty added by predicting the state parameters one-step ahead.

The one-step forecasting distribution of observation $P(y_{t+1} \mid D_t) \sim N(f_{t+1}, Q_{t+1})$ can be obtained from the observation equation (Equation 1) as

$$f_{t+1} = E[y_{t+1}|D_t] = F_{t+1}'a_{t+1}; Q_{t+1} = Var[y_{t+1}|D_t] = F_{t+1}'R_{t+1}F_{t+1} + V_{t+1}, \tag{4}$$

where V_{t+1} represents the extra uncertainty added by predicting the observation one-step ahead.

As time moves forward, once the new observation y_{t+1} is available at time t+1, the posterior distribution of the state parameters can be updated to $P(\theta_{t+1}|\ D_{t+1}) \sim N(m_{t+1},\ C_{t+1})$ in which the mean and variance are given by

$$m_{t+1} = a_{t+1} + A_{t+1}e_{t+1}; C_{t+1} = R_{t+1} - A_{t+1}A_{t+1}^T Q_{t+1}, \tag{5}$$

$$e_{t+1} = y_{t+1} - f_{t+1}; A_{t+1} = \frac{R_{t+1}F_{t+1}}{Q_{t+1}}, \tag{6}$$

where $D_{t+1} = \{D_t, y_{t+1}\}$. Note that A_{t+1} is the adaptive coefficient, which can be viewed as the information tuner and e_{t+1} is the one-step forward forecast error, which is the difference between the observed value y_{t+1} and its expectation f_{t+1}.

Figure 1 illustrates the flowchart of BDLM inference and forecasting.[28] After obtaining the posterior distribution $P(\theta_{t+1}|\ D_{t+1})$, the observation at t+2 can be predicted, and so on. Analytical solution in terms of Equation 5 for this process is usually impossible or intractable. Rather, MCMC simulation procedures provide a more rational route to gain an approximate solution. The Gibbs sampler, one of the MCMC methods, detailed in Section 3, will be executed to obtain such an approximate solution in view of the availability of a full set of conditional distribution for sampling.

It is apparent that the covariance matrices of the process noise W_t and the measurement noise V_t should be prescribed. Improper assignment of these two covariance matrices might lead to unreliable estimation and misleading uncertainty estimation on the state parameters. In order to resolve this problem, efforts have been devoted to the development of methods to estimate the noise parameters. The methods can be classified into three categories: covariance matching, correlation, and Bayesian techniques.[35,36] In this study, the Bayesian technique will be employed to formulate the posterior distribution of the noise parameters with which the uncertainty of noise parameters can further be quantified. The detailed solution procedures will be presented in Section 3.

2.2 | Model components for forecasting

Long-term SHM data, especially long-term strain monitoring data, are in general influenced by trend, seasonal (cyclical), and regression effects. In this study, DLMs that enable the modeling of trend, seasonal (cyclical), and regression effects are formulated in the Bayesian context. When taking into account the trend, seasonal (cyclical), and regression effects, the observation y_t can be expressed as

$$y_t = y_{Tt} + y_{St} + y_{Rt} + v_t, \tag{7}$$

where y_{Tt}, y_{St}, y_{Rt}, and v_t stand for the trend component, seasonal (cyclical) component, regression component (including the autoregression component), and measurement error (refer to v_t in Equation 1), respectively. An extended DLM accounting for these effects can be obtained by defining the following parameters in Equations 1 and 2.

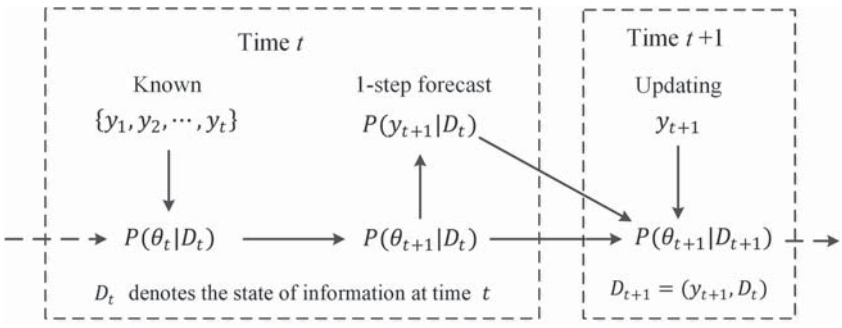

FIGURE 1 Flowchart of BDLM inference and forecasting

$$\theta_t = \begin{pmatrix} \theta_{Tt} \\ \theta_{St} \\ \theta_{Rt} \end{pmatrix}; F_t = \begin{pmatrix} F_{Tt} \\ F_{St} \\ F_{Rt} \end{pmatrix}; G_t = \begin{pmatrix} G_{Tt} & & \\ & G_{St} & \\ & & G_{Rt} \end{pmatrix}; W_t = \begin{pmatrix} W_{Tt} & & \\ & W_{St} & \\ & & W_{Rt} \end{pmatrix}; V_t = \sigma_{obs}^2. \tag{8}$$

2.2.1 | Trend component

Trends in the monitoring data time series, viewed as a smooth evolution over time, can be modeled by a polynomial function.

The simplest trend model is the first-order polynomial trend, which can be expressed as

$$y_t = \theta_{t,1} + v_t,\ v_t \tilde{N}\left(0, \sigma_{obs}^2\right), \tag{9}$$

$$\theta_{t,1} = \theta_{t-1,1} + \omega_{t,1}, \omega_{t,1} \tilde{N}\left(0, \sigma_1^2\right). \tag{10}$$

A second-order polynomial trend provides a linear growth model, which has the form

$$y_t = \theta_{t,1} + v_t, v_t \tilde{N}\left(0, \sigma_{obs}^2\right), \tag{11}$$

$$\theta_{t,1} = \theta_{t-1,1} + \theta_{t-1,2} + \omega_{t,1}, \omega_{t,1} \tilde{N}\left(0, \sigma_1^2\right), \tag{12}$$

$$\theta_{t,2} = \theta_{t-1,2} + \omega_{t,2},\ \omega_{t,2} \tilde{N}\left(0, \sigma_2^2\right). \tag{13}$$

Similarly, general higher-order polynomial models take the form[28]

$$y_t = \theta_{t,1} + v_t,\ v_t \tilde{N}\left(0, \sigma_{obs}^2\right), \tag{14}$$

$$\theta_{t,j} = \theta_{t-1,j} + \theta_{t-1,j+1} + \omega_{t,j}, \omega_{t,j} \tilde{N}\left(0, \sigma_j^2\right), (\ j = 1, ..., n-1), \tag{15}$$

$$\theta_{t,n} = \theta_{t-1,n} + \omega_{t,n}, \omega_{t,n} \tilde{N}\left(0, \sigma_n^2\right),\ (\ j = n), \tag{16}$$

in which $\theta_{t,1}$ is the level at time t that between times $t-1$ and t changes by addition of $\theta_{t-1,2}$ plus the noise $\omega_{t,1}$; $\theta_{t-1,2}$ represents a systematic change in level that itself changes by the addition of $\theta_{t-1,3}$ plus noise. Proceeding through the state parameters for $j = 1,...,n-1$, each $\theta_{t,j}$ changes systematically via the increment $\theta_{t-1,j+1}$ and the additional noise term $\omega_{t,j}$. The nth component $\theta_{t,n}$ changes stochastically.

In terms of the state-space form, the higher-order polynomial models can be written as

$$\theta_{Tt} = (\theta_{t,1}, ..., \theta_{t,n})'; F_{Tt} = (1, 0, 0, ..., 0)', \tag{17}$$

$$G_{Tt} = \begin{pmatrix} 1 & 1 & 0 & \cdots & 0 \\ 0 & 1 & 1 & \cdots & 0 \\ 0 & 0 & 1 & \cdots & 0 \\ \vdots & \vdots & \vdots & \ddots & \vdots \\ 0 & 0 & 0 & \cdots & 1 \end{pmatrix}; W_{Tt} = diag\left(\sigma_1^2, \cdots \sigma_n^2\right); V_t = \sigma_{obs}^2. \tag{18}$$

In practice, low-order (e.g., first- or second-order) polynomial models are often employed to express the trend in time series response data, yet higher-order models are rarely used.

2.2.2 | Seasonal (cyclical) component

Seasonal (cyclical) behavior, such as daily variation and seasonal variation, is evident in various time series data associated with structural systems. For example, the displacement of bridge expansion joints changes periodically every day. It is important to perceive and reflect seasonal (cyclical) patterns in forecasting models. The seasonal (cyclical) behavior of time series can be satisfactorily modeled using harmonic functions, such as sines and cosines.[37]

Consider the time series y_t represented by n harmonics as

$$y_t = \sum_{k=1}^{n} (a_k \cos(k\omega t) + b_k \sin(k\omega t)) + v_t, \tag{19}$$

where $\omega = 2\pi/s$, s is the period of the cyclical pattern; a_k and b_k correspond to the amplitude of periodic component; v_t is the observation error.

The simplest seasonal (cyclical) model is involving only one harmonic function, which can be expressed in state-space form as[28]

$$\theta_{St} = \left(u_{t,1}, u_{t,1}^*\right)'; F_{St} = (1,0)'; G_{St} = \begin{pmatrix} \cos\omega & \sin\omega \\ -\sin\omega & \cos\omega \end{pmatrix}; W_{St} = \begin{pmatrix} \sigma_{s,1}^2 & 0 \\ 0 & \sigma_{s,1}^2 \end{pmatrix}, \tag{20}$$

with

$$u_{t,1} = a_1 \cos(\omega t) + b_1 \sin(\omega t); u_{t,1}^* = -a_1 \sin(\omega t) + b_1 \cos(\omega t). \tag{21}$$

Increasing the number of harmonics amounts to increasing the complexity of seasonal component. A DLM with n harmonics can be expressed as

$$\theta_{St} = \left(u_{t,1}, u_{t,1}^*, u_{t,2}, u_{t,2}^*, ..., u_{t,n}, u_{t,n}^*\right)'; F_{St} = (1,0,1,0,...,0)', \tag{22}$$

$$G_{St} = diag(G_{St,1}, \cdots, G_{St,n}); W_{St} = diag(W_{St,1}, \cdots, W_{St,n}), \tag{23}$$

with

$$u_{t,k} = a_k \cos(k\omega t) + b_k \sin(k\omega t); u_{t,k}^* = -a_k \sin(k\omega t) + b_k \cos(k\omega t), \tag{24}$$

$$G_{St,k} = \begin{pmatrix} \cos k\omega & \sin k\omega \\ -\sin k\omega & \cos k\omega \end{pmatrix}; W_{St,k} = \begin{pmatrix} \sigma_{s,k}^2 & 0 \\ 0 & \sigma_{s,k}^2 \end{pmatrix}. \tag{25}$$

2.2.3 | Regression component

The regression effect can be modeled only when the regressor(s) are observed (measured) together with the response variable(s). When the time series response data are in regression with q independent variables $\{x_1, x_2, \cdots, x_q\}$, we have

$$y_t = \beta_{t,1} x_{t,1} + \cdots + \beta_{t,q} x_{t,q} + v_t, \tag{26}$$

$$\beta_{t,i} = \beta_{t-1,i} + \omega_{t,i}, \omega_{t,i} \tilde{N}\left(0, \sigma_i^2\right) (i = 1, \cdots, q), \tag{27}$$

which correspond to the DLM with the following parameters:

$$\theta_{Rt} = \left(\beta_{t,i}, \cdots, \beta_{t,q}\right)'; F_{Rt} = \left(x_{t,1}, \cdots, x_{t,q}\right)'; G_t = I_q; W_{Rt} = diag\left(\sigma_1^2, \cdots \sigma_q^2\right). \tag{28}$$

3 | SIMULATION-BASED BAYESIAN INFERENCE: GIBBS SAMPLER

For a given BDLM, the main task is to estimate the unobserved state parameters and hyperparameters and make predictions on future structural responses based on the acquired structural response time series. From a Bayesian perspective, estimation and forecasting are achieved by computing the posterior distributions of interest. Conditional on prior information and available structural responses through time T, beliefs about the future can be expressed by the joint posterior distribution as

$$p\left(y^{T+1:T+H}, \theta^{T+1:T+H}, \theta^{1:T}, \psi | y^{1:T}\right), \tag{29}$$

where $y^{T+1:T+H}$ and $\theta^{T+1:T+H}$ represent the future structural responses and state parameters from time T onward to (T+H), respectively; $y^{1:T}$ and $\theta^{1:T}$ represent the history of observed structural responses and state parameters up to time T; and $\psi = \left(\sigma_y^2, \sigma_{\theta,1}^2, \sigma_{\theta,2}^2, \cdots, \sigma_{\theta,p}^2\right)$ are hyperparameters, where σ_y^2 is the unknown observation variance (refer to V_t in Equation 1), and $\sigma_{\theta,1}^2, \sigma_{\theta,2}^2, \cdots, \sigma_{\theta,p}^2$ are the evolution variances (refer to $W_t$in Equation 2). Despite complicated in manipulation, the above expression (Equation 29) can be decomposed into tractable components as

$$p\left(y^{T+1:T+H}, \theta^{T+1:T+H}, \theta^{1:T}, \psi | y^{1:T}\right) = p\left(\theta^{1:T}, \psi | y^{1:T}\right) \times p\left(y^{T+1:T+H}, \theta^{T+1:T+H} | \theta^{1:T}, \psi\right). \tag{30}$$

This expression decomposes the joint distribution into two parts: The first part, $p(\theta^{1:T},\psi|\, y^{1:T})$, is the joint posterior density for the history of the state parameters and hyperparameters; and the second part, $p(y^{T+1:T+H},\theta^{T+1:T+H}|\, \theta^{1:T},\psi)$, is the joint distribution for future structural responses and state parameters based on the current state parameters and hyperparameters. An analytical solution for each part is impossible, even for simple cases. Therefore, the Gibbs sampler, one of the MCMC methods, is employed to explore the posterior distribution. According to the components shown in Equation 30, the algorithm is split into two steps: (i) Draw a pair of ($\theta^{1:T}$, ψ) from $p(\theta^{1:T},\psi|\, y^{1:T})$(see Section 3.1), and (ii) plug the draw into $p(y^{T+1:T+H},\theta^{T+1:T+H}|\, \theta^{1:T},\psi)$ to generate the future state parameters $\theta^{T+1:T+H}$ and structural responses $y^{T+1:T+H}$ (see Section 3.2).

3.1 | Estimation of BDLM parameters

The posterior distribution for the state parameters $\theta^{1:T}$ and hyperparameters ψ can be decomposed into

$$p\left(\theta^{1:T}, \psi | y^{1:T}\right) = p\left(\theta^{1:T} | \psi, y^{1:T}\right) p\left(\psi | y^{1:T}\right). \tag{31}$$

The Gibbs sampler for posterior evaluation iterates the following two steps: (i) Draw state parameters from $p(\theta^{1:T}|\, \psi, y^{1:T})$ conditional on the observed structural responses and hyperparameters; and (ii) draw hyperparameters from $p(\psi|\, \theta^{1:T}, y^{1:T})$ conditional on the observed structural responses and state parameters. Subject to regularity conditions,[38] the sequence of draws, $\theta_i^{1:T},\psi_i$ (i = 1,2,...N), converge to a draw from the joint distribution $p(\theta^{1:T},\psi|\, y^{1:T})$.

In a Bayesian setting, we need to specify a prior distribution for the state parameters and hyperparameters. One popular choice of the prior distribution is conjugate normal inverse gamma, that is, normal distribution for the state

parameters and inverse gamma distribution for the hyperparameters.[39,40] As the hyperparameters (including the unknown observation variance V_t and evolution variance W_t) are non-negative, the inverse gamma distribution describing the continuous probability distributions on the positive real line is perfectly suited for the hyperparameters.[41]

$$P(\theta_0|\psi_0) \propto N(\bar{\theta},\bar{P}); P(\psi_0) \propto IG\left(T_0,\bar{\psi}^{-1}\right), \tag{32}$$

where $\bar{\theta}$ and $\bar{P}$ are the mean and variance of the normal distribution; T_0 and $\bar{\psi}^{-1}$ are the shape and scale parameters of the inverse gamma distribution.

3.1.1 | Gibbs step 1: Drawing state parameters given hyperparameters

A key task is the generation of samples from the distribution $p(\theta^{1:T}|\ \psi, y^{1:T})$. The forward filtering backward sampling (FFBS) algorithm[42] provides an easy way of generating independent samples. Forward filtering (Kalman filtering) can update the BDLM based on the observed data, and backward sampling (Kalman smoothing) can retrospectively reconstruct the behavior of the system concerning its underlying information. Note that FFBS is formalized as a building block of a Gibbs sampler.

The conditional density $p(\theta^{1:T}|\ \psi, y^{1:T})$ in the first part of Equation 31 can be factored as[43]

$$p(\theta^{1:T}|\psi,y^{1:T}) = p\left(\theta_T|\psi,y^{1:T}\right)\prod_{t=1}^{T-1} p\left(\theta_t|\theta_{t+1},\psi,y^{1:T}\right). \tag{33}$$

The first term $p(\theta_T|\ \psi,y^{1:T})$ is the marginal posterior distribution for the terminal state, and the other terms are conditional distributions for the preceding time instants. Because the distributions on the right-hand side of the expression conform to Gaussian, the samples can be separately drawn from Equation 34.

$$p\left(\theta_T|\psi,y^{1:T}\right)\tilde{N}\left(\theta_{T|T},P_{T|T}\right); p\left(\theta_t|\theta_{t+1},\psi,y^{1:T}\right)\tilde{N}\left(\theta_{t|t+1},P_{t|t+1}\right). \tag{34}$$

1. Mean and variance of $p(\theta_T|\ \psi,y^{1:T})$

The mean $\theta_{T|T}$ and variance $P_{T|T}$ can be obtained via the forward filtering (Kalman filtering), which is a recursive algorithm by estimating the state parameters given information up to the current time. The algorithm includes the following equations that are evaluated recursively over time. Starting from initial values $\theta_{0|0}$ and $P_{0|0}$, the conditional means and variances can be obtained by iteration[43]

$$\theta_{t|t-1} = G_t\theta_{t-1|t-1}; P_{t|t-1} = P_{t-1|t-1} + W; \eta_{t|t-1} = y_t - F_t'\theta_{t|t-1}, \tag{35}$$

$$f_{t|t-1} = F_t'P_{t|t-1}F_t + V; \theta_{t|t} = \theta_{t|t-1} + K_t\eta_{t|t-1}; P_{t|t} = P_{t|t-1} - K_tF_t'P_{t|t-1}, \tag{36}$$

where $K_t = P_{t|t-1}F_tf_{t|t-1}^{-1}$. The first part of Equation 35 predicts state parameters one-step ahead using the transition equation, and the) second part of Equation 35 estimates the variance of state parameters at time t given the information at time $t-1$. The third part of Equation 35 and first part of Equation 36 calculate the mean and variance of the prediction error, respectively. The final two 35) parts of Equation 36 are applied to update state parameters using the new observation y_t at time t. Executing these equations for instants $t = 1,2...,T$, the final recursion yields $\theta_{T|T}$ and $P_{T|T}$ for the terminal state.

2. Mean and variance of $p(\theta_t|\ \theta_{t+1},\psi,y^{1:T})$

After the terminal state θ_T has been drawn from $p(\theta_T|\ \psi,y^{1:T})$, the next task is to recursively draw θ_t(for $t = T-1$, $T-2$,...,0) from $p(\theta_t|\ \theta_{t+1},\psi,y^{1:T})$ by the backing sampling (Kalman smoothing). Assuming that (θ_T, ..., θ_{t+1}) have

already been obtained, the next step is to draw θ_t from $N(\theta_{t|t+1}, P_{t|t+1})$, where $\theta_{t|t+1}$ and $P_{t|t+1}$ can be computed by iteration

$$\theta_{t|t+1} = \theta_{t|t} + P_{t|t}P^{-1}_{t+1|t}\left(\theta_{t+1} - \theta_{t|t}\right); P_{t|t+1} = P_{t|t} - P_{t|t}P^{-1}_{t+1|t}P_{t|t}. \tag{37}$$

Note that $\theta_{t|t+1}$ explicitly depends on the value of θ_{t+1} already generated. The implementation procedure of the FFBS algorithm is summarized in Algorithm 1.

Algorithm 1. Forward filtering backward sampling (FFBS)

1. Run Kalman filter; 2. Draw $\theta_T \sim N(\theta_{T|T}, P_{T|T})$; 3. For $t = T-1, T-2, \ldots, 0$, draw $\theta_t \sim N(\theta_{t|t+1}, P_{t|t+1})$

In summary, the Gibbs sampler for drawing state parameters involves three steps. First, draw θ_T from the first part of Equation 34, in conjunction with using Equations 35 and 36 to compute the mean and variance. Next draw θ_{T-1} from the second part of Equation 34 in conjunction with using Equation 37 to compute the mean and variance conditional on θ_T. Then draw θ_{T-2} conditional on the realization of θ_{T-1} until arrival at the beginning of the sample.

3.1.2 | Gibbs step 2: Drawing hyperparameters given state parameters

Conditional on $\theta^{1:T}$ and $Y^{1:T}$, the hyperparameters are observable. Because the prior of ψ is an inverse Gamma distribution and the conditional likelihood is Gaussian, the posterior is also an inverse Gamma distribution

$$p\left(\psi|\theta^{1:T}, y^{1:T}\right) = IG\left(T_1, \psi_1^{-1}\right), \tag{38}$$

where

$$T_1 = T_0 + \frac{T}{2}; \psi_1 = \bar{\psi} + \frac{1}{2}\bar{V}_T; \bar{V}_T = diag\left(SS_y, SS_{\theta,1}, \cdots, SS_{\theta,p}\right), \tag{39}$$

$$SS_y = \sum_{t=1}^{T}\left(y_t - F_t'\theta_t\right)^2; SS_{\theta,i} = \sum_{t=1}^{T}\left(\theta_{t,i} - \left(G_t\theta_{t-1}\right)_i\right)^2,\ i = 1, \cdots, p, \tag{40}$$

3.2 | Forecast about the future

Having processed the known data, the next task is to simulate the future state parameters and observations. Conditional on the current state parameters and hyperparameters, the joint posterior density for future observations and state parameters is quite traceable by factoring it into

$$p\left(y^{T+1:T+H}, \theta^{T+1:T+H}|\theta_T, \psi, y^{1:T}\right) = p\left(\theta^{T+1:T+H}|\theta_T, \psi, y^{1:T}\right) \times p\left(y^{T+1:T+H}|\theta^{T+1:T+H}, \theta_T, \psi, y^{1:T}\right), \tag{41}$$

in which the first term on the right-hand side is a marginal distribution of future state parameters, and the second term is a conditional distribution of future observations. Because the state parameters are Markov, the first term is further factored into

$$p\left(\theta^{T+1:T+H}|\theta_T, \psi, y^{1:T}\right) = \prod_{i=1}^{H} p\left(\theta_{T+i}|\theta_{T+i-1}, \psi, y^{1:T}\right), \tag{42}$$

where $p(\theta_{T+i}|\theta_{T+i-1}, \psi, y^{1:T}) \sim N(\theta_{T+i-1}, W)$. Therefore, to sample future state parameters from 41 Equation 42, H random draws of ω_i are taken from $N(0, W)$ and iterate on the system equation

$$\theta_{T+i} = \theta_{T+i-1} + \omega_i. \tag{43}$$

Having obtained the future state parameters, all that remains is to forecast future observations. The second term in 40 Equation 41 can be factored as

$$p\left(y^{T+1:T+H}|\theta^{T+1:T+H},\theta_T,\psi,y^{1:T}\right) = \prod_{i=1}^{H} p\left(y_{T+i}|y^{T:T+i-1},\theta^{T+1:T+H},\theta_T,\psi,y^{1:T}\right), \tag{44}$$

where $p\left(y_{T+i}|y^{T+1:T+i-1},\theta^{T+1:T+H},\theta_T,\psi,y^{1:T}\right)\tilde{N}\left(F'_{T+i}\theta_{T+i},V\right)$. To sample future observation from Equation 44, H random draws of v_i are taken from $N(0,V)$ and then the future observation site rate on the measurement equation

$$y_{T+i} = F'_{T+i}\theta_{T+i} + v_i. \tag{45}$$

4 | BMCS FOR BDLM

One commonly encountered problem in regression modeling lies in finding the best/optimal model class suitable for exploring the relationships between the response variables (e.g., structural strain response) and explanatory variables (e.g., the trend, seasonal, and temperature effect) and amenable to forecasting. Although a more complicated model class can fit the data more accurately than one less complicated, it is likely to lead to overfitting. When an overfitted model class is used for future prediction, it would yield poor results because the identified model class depends heavily on the training data and also the measurement noise inherent in the data. Thus, the formulated model class should balance accuracy against complexity. In the Bayesian framework, the concept of model class selection has been addressed by Yuen.[39] More details on BMCS and its practical implementations can be found in the literature.[9,16]

The goal of BMCS is to use the information in the observed data $y^{1:T}$, to select the most plausible model class, which represents the observed physical phenomenon among a set of model class candidates C_j ($j = 1,2,...,N_c$). For the sake of brevity, the term $y^{1:T}$ is denoted as y in this section. The model with maximum posterior probability $p(y)$ is selected as the one most plausible. For each candidate model C_j, the posterior distribution of model parameters (ϑ) is defined via Bayes' theorem

$$p(\vartheta|y) = \frac{p(y|\vartheta)p(\vartheta)}{p(y)}, \tag{46}$$

where $p(y|\vartheta)$ and $p(\vartheta)$ are the likelihood function and joint prior distribution, respectively; $p(y)$ is the marginal likelihood that we desire to compute. The marginal likelihood in log format is

$$ln\,p(y) = ln\,p(y|\vartheta) + ln\,p(\vartheta) - ln\,p(\vartheta|y). \tag{47}$$

When the three terms on the right hand-side of Equation 47 are analytically available, the marginal likelihood, $lnp(y)$, can be computed readily. However, the third term $p(\vartheta|y)$ is often difficult to calculate because of the unknown exact form of the posterior distribution. In this connection, Chib[44] proposed to divide the parameter vector ϑ into several blocks so that the full conditional distribution for each block is available in closed form. To illustrate this idea, the case of two blocks is considered here as an example, that is, $\vartheta = (\theta,\psi)$, where $p(\theta|\psi,y)$ and $p(\psi|y)$ are available in closed form. The joint posterior distribution of ϑ can be estimated as

$$p(\vartheta|y) = p(\theta,\psi|y) = p(\theta|\psi,y)p(\psi|y), \tag{48}$$

where an appropriate Monte Carlo estimate for $p(\psi|y)$ is

$$\hat{p}(\psi|y) \approx \frac{1}{L_1}\sum_{k=1}^{L_1} f\left(\psi|y,\theta^{(k)}\right), \tag{49}$$

in which $\{\theta^{(k)}; k = 1, \cdots, L_1\}$ is a set of posterior samples derived using the Gibbs sampler. The term $\hat{p}(\psi|y)$ tends to $p(\psi|y)$ as L_1 becomes large. Thus, the marginal likelihood can be estimated as

$$\ln p(y) \approx \ln p(y|\theta^\star,\psi^\star) + \ln p(\theta^\star,\psi^\star) - \ln p(\theta^\star|\psi^\star,y) - \ln \hat{p}(\psi^\star|y), \tag{50}$$

where the first three terms on the right-hand side are available in closed form. The value of $\theta^\star,\psi^\star$ might be chosen as the posterior mean, posterior mode, posterior median, or other pointsall of which maximize the accuracy of this approximation. The maximum of *ln p*(*y*) (denoted as LLH) is favored.

Figure 2 illustrates the flowchart of the proposed method integrating the parameter estimation, model class selection, and forecasting. First, the parameters of each candidate DLM (C_j) with different components are estimated by Gibbs sampler. Then the maximum LLH of each model class is calculated by BMCS to determine the optimal one in representing the observations. Finally, one- or multistep ahead predictions are pursued in terms of the optimal model class.

5 | FORECAST OF STRAIN RESPONSE OF TING KAU BRIDGE

5.1 | TKB and SHM system

The Ting Kau Bridge (TKB) in Hong Kong is a three-tower cable-stayed bridge with two main spans of 448 and 475 m and two side spans of 127 m each. The bridge deck is separated into two carriage ways, each of width 18.8 m. Between them are three slender single-leg towers with heights of 170, 194, and 158 m, respectively. The deck is supported by 384 stay cables in four cable planes.

To ensure the operation safety of the bridge, a sophisticated long-term SHM system, named WASHMS, had been devised and implemented by the Hong Kong SAR Highway Department to monitor the structural health and conditions of TKB.[2,45,46] As the focus of this study is on the forecast of structural strain responses, we concern only the deployment of strain gauges and the relevant sensors. As part of the long-term SHM system installed on TKB, a total of 88 strain gauges (66 single strain gauges and 22 rosette strain gauges) were deployed to monitor strain response at four bridge

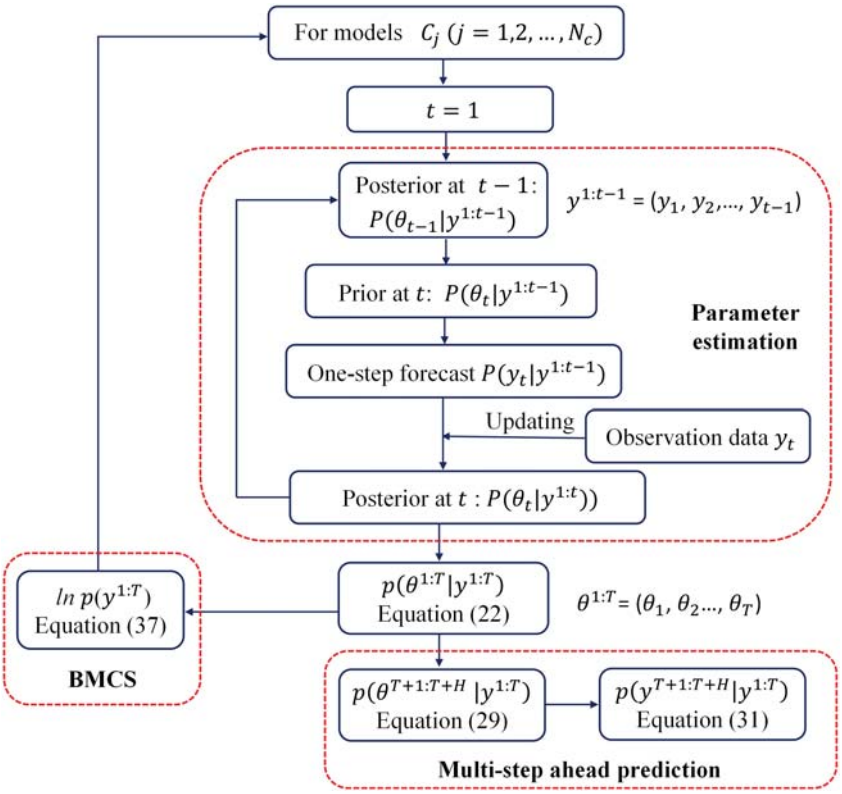

FIGURE 2 Schematic framework of the proposed method

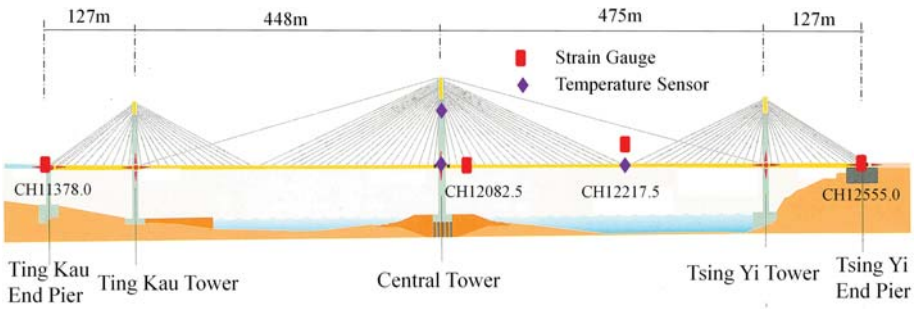

FIGURE 3 Location of strain gauges and temperature sensors along bridge deck

deck cross sections denoted CH113782.0, CH12082.5, CH12217.5, and CH12555.0 (see Figure 3). Likewise, 83 temperature sensors were installed at one bridge deck cross section and two bridge tower cross sections to measure the temperature in steel, concrete, asphalt, and environmental air. Figures 4 and 5 show the layout of strain gauges and temperature sensors on the bridge deck cross section CH12217.5.The sampling rates of the strain gauges and temperature sensors are 25.6 and 0.07 Hz, respectively.

Without loss of generality, the strain gauge SS-GLW-06 located at the cross section CH12217.5 shown in Figure 3 is chosen to illustrate the proposed Bayesian real-time forecast approach. In the present study, the real-time monitoring data (including strain and temperature) collected during a period of 27d are of concern. To decrease the uncertainties arising from the measurement facilities, the average hourly strain responses and temperature are used as the target quantities. As a result, a total of 648 observations are formed from 24 values per day. Figure 6a shows the time history of the averaged strain responses. It is seen that the strain responses exhibit a daily cyclical feature, implying that a seasonal (cyclical) component should be incorporated in modeling. Figure 6b shows the averaged temperatures of structural steel (P1-GLE-02A, P1-GLE-02B, and P1-GLE-02C), atmosphere (P3-GLE-02A), and asphalt (P4-GLE-02) for the same time period. Similar to the strain responses, the temperatures are also periodical, which would be the reason causing the daily cyclical strain responses.

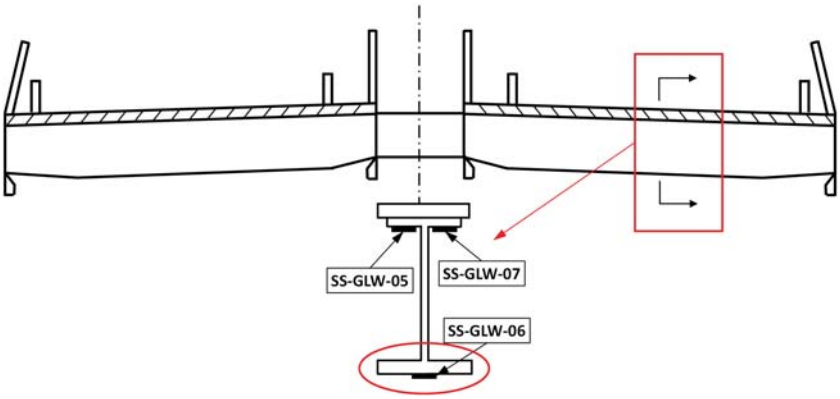

FIGURE 4 Layout of strain gauges on deck cross section CH12217.5

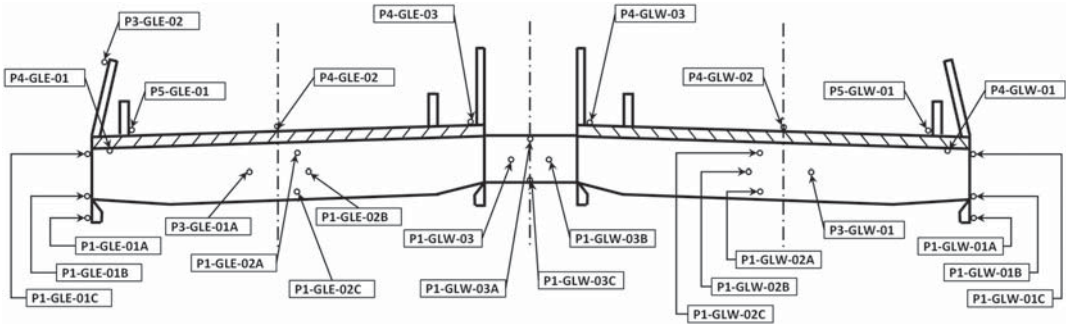

FIGURE 5 Layout of temperature sensors on deck cross section CH12217.5

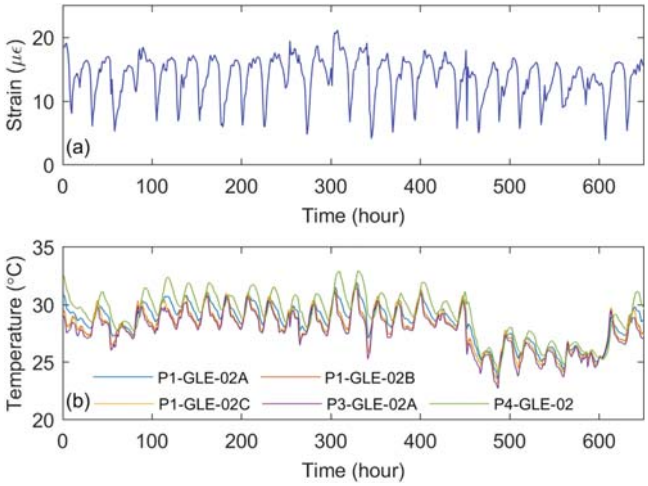

FIGURE 6 Time histories of strain and temperature monitoring data: (a) strain; (b) temperature

5.2 | Comparison of forecast accuracy

In the present work, we will address monitoring-based modeling, inference, and forecasting of the strain responses by evaluating and comparing the following cases: (i) the DLM taking account of trend and seasonal (cyclical) effect only; (ii) the DLM taking account of trend and regression effect only; and (iii) the DLM taking account of trend, seasonal (cyclical), and regression effects concurrently. To comprehensively assess the forecasting performance, both one-step and multistep ahead predictions are explored.

The forecasting performance of each model class is evaluated by comparing the predicted strain responses with the measured counterparts and quantifying the forecasting uncertainty. As visual discrimination is more or less subjective, performance metrics that allow for evaluating the forecasting capabilities quantitatively are desired. Apart from the LLH (i.e., $ln\ p(y)$) estimated by BMCS in Section 4, other two common statistics indicators, root mean squared error (RMSE) and mean absolute percentage error (MAPE), are also adopted to validate the accuracy of prediction, defined as

$$RMSE = \sqrt{\frac{\sum_{t=1}^{T}(\hat{y}_t - y_t)^2}{T}}, \tag{51}$$

$$MAPE = \frac{1}{T}\sum_{t=1}^{T}\left|\frac{\hat{y}_t - y_t}{y_t}\right|, \tag{52}$$

where $\hat{y}_t$ and y represent the predicted and observed values, respectively, at time t, and T is the number of observations.

5.2.1 | Model 1: Trend and seasonal (cyclical)

In the first model class, only the trend and seasonal (cyclical) effects are considered in the DLM for structural strain response,

$$y_t = y_{Tt} + y_{St} + v_t. \tag{53}$$

A crucial issue associated with this model class is the choice of the proper polynomial order for the trend component and harmonics for the seasonal (cyclical) component. The polynomial order affects the sensitivity of trend effect; that is, the higher the order, the more dramatic the trend variation. In practice, a second-order polynomial model (linear trend) is generally suitable for simulating the trend effect.[47] In this regard, the DLMs by considering a second-order

polynomial function for the trend component and different harmonics for the seasonal (cyclical) component are explored. That is,

Model 1a:	Linear trend + one harmonic;
Model 1b:	Linear trend + two harmonics;
Model 1c:	Linear trend + three harmonics;
Model 1d:	Linear trend + four harmonics.

With the obtained LLH values listed in Table 1, Model 1c with three harmonics is identified to be the one most plausible. The RMSE and MAPE scores also prove that Model 1c gives the best forecast.

The results from Model 1c are demonstrated in Figure 7. Figure 7a shows the real observed data together with 1-step ahead prediction and the corresponding 90% prediction interval. Generally, most of the observations lie within the predictive interval except for some extrema. The forecast performance is satisfactory. In Figure 7b, the results of trend analysis with 90% probability envelope are plotted. The level remains relatively stable and, to an extent, reflects the trend of change. Figure 7c shows the seasonal (cyclical) component with 90% credibility interval. Apparently, it varies with time but very slowly. To have a clear picture of the prediction performance, the prediction residuals are shown in Figure 7d–f. Figure 7d shows the scaled prediction errors with 90% probability interval (red dashed line). Obviously, the majority of the prediction errors are within the probability region. In Figure 7e, the autocorrelation function of the prediction errors is plotted. It is seen that the residuals are not completely uncorrelated, as relative autocorrelations exist at some lags. Figure 7f gives the Quantile–Quantile (Q–Q) plot of the prediction errors, which compares the empirical quantiles of the prediction errors with those obtained from the theoretical distribution. The results show that the points (normalized error values) approximately lie on the line of expectation.

5.2.2 | Model 2: Trend and regression

In the second model class, only the trend and regression effects are considered in the DLM for structural strain response,

$$y_t = y_{Tt} + y_{Rt} + v_t, \tag{54}$$

where a two-order polynomial model (linear trend) is used to simulate the trend effect, and temperature as an explanatory variable is applied to model the regression effect.

Temperature in a bridge deck cross section can be decomposed into two portions: differential temperature and effective temperature. The differential temperature is the difference in temperature between the upper and lower surfaces of the bridge deck cross section, which causes internal stresses and bending moments; whereas the effective temperature is the average temperature distributed along the section, which results in longitudinal movements of the bridge deck.[48] Hence, it is necessary to try two different model versions according to the temperature category. For Model 2a, the

TABLE 1 Summary of forecast performance for different models

Model no.	RMSE	MAPE (%)	LLH
Model 1a	1.69	10.77	−666.74
Model 1b	1.69	10.78	−665.73
Model 1c	1.42	9.05	−419.17
Model 1d	1.72	10.93	−652.63
Model 2a	2.12	13.71	−948.60
Model 2b	2.25	14.81	−1154.01
Model 3	1.40	8.71	−400.01

Abbreviations: MAPE, mean absolute percentage error; RMSE, root mean squared error.

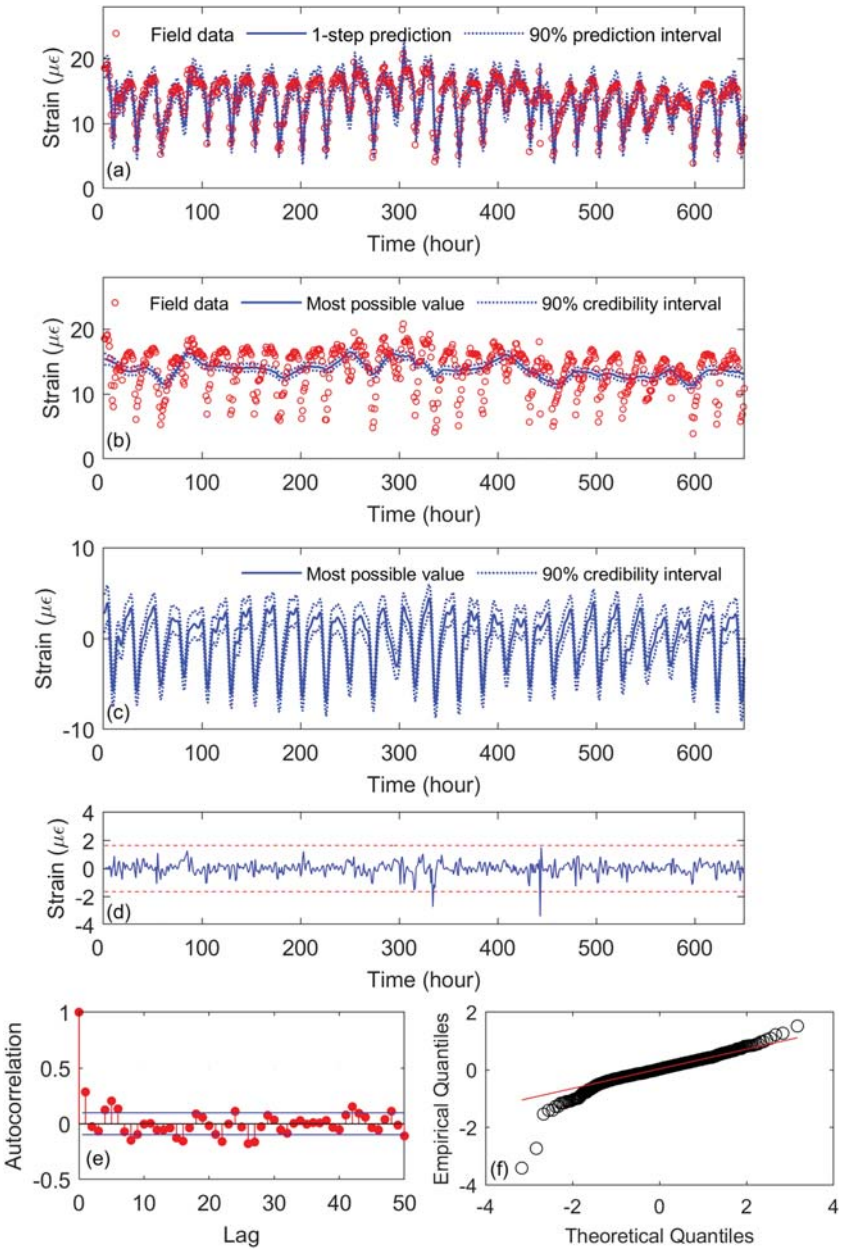

FIGURE 7 Model 1c: linear trend + 3 harmonics: (a) one-step ahead prediction; (b) trend component; (c) seasonal (cyclical) component; (d) scaled forecast residuals; (e) autocorrelation of forecast residuals; (f) Q–Q plot of forecast residuals

differential temperature is regarded as an explanatory variable, whereas Model 2b makes use only of the data obtained from the temperature sensor (P1-GLE-02C) close to the strain gauge (SS-GLW-06).

The values of the three criteria listed in Table 1 show that Model 2a achieves slightly better predictions than Model 2b. The results of Model 2a are presented in Figure 8. Apparently, the one-step ahead predictions of Model 2a in Figure 8a are not better than those of Model 1c in Figure 7a, especially the prediction of extreme observations, which are also reflected by the values of LLH, RMSE, and MAPE. Compared with Model 1c, the trend component of Model 2a shown in Figure 8b fluctuates more and does not match well the underlying trend of structural strain response. Figure 8c shows the regression component with differential temperature as an explanatory variable. It is evident that the regression component also bears the seasonal (cyclical) properties. The standardized prediction errors of Model 2a (Figure 8d) are visibly larger than thoseof Model 1c, and there are more errors beyond the 90% probability interval. Again, it can be found from Figure 8e that the autocorrelation function of prediction errors has the cyclical characteristics with 24 points per cycle, which means that the periodic term has not been well removed. The results of the Q–Q plot for prediction errors (Figure 8f) demonstrate that the residuals are not very consistent with a normal distribution.

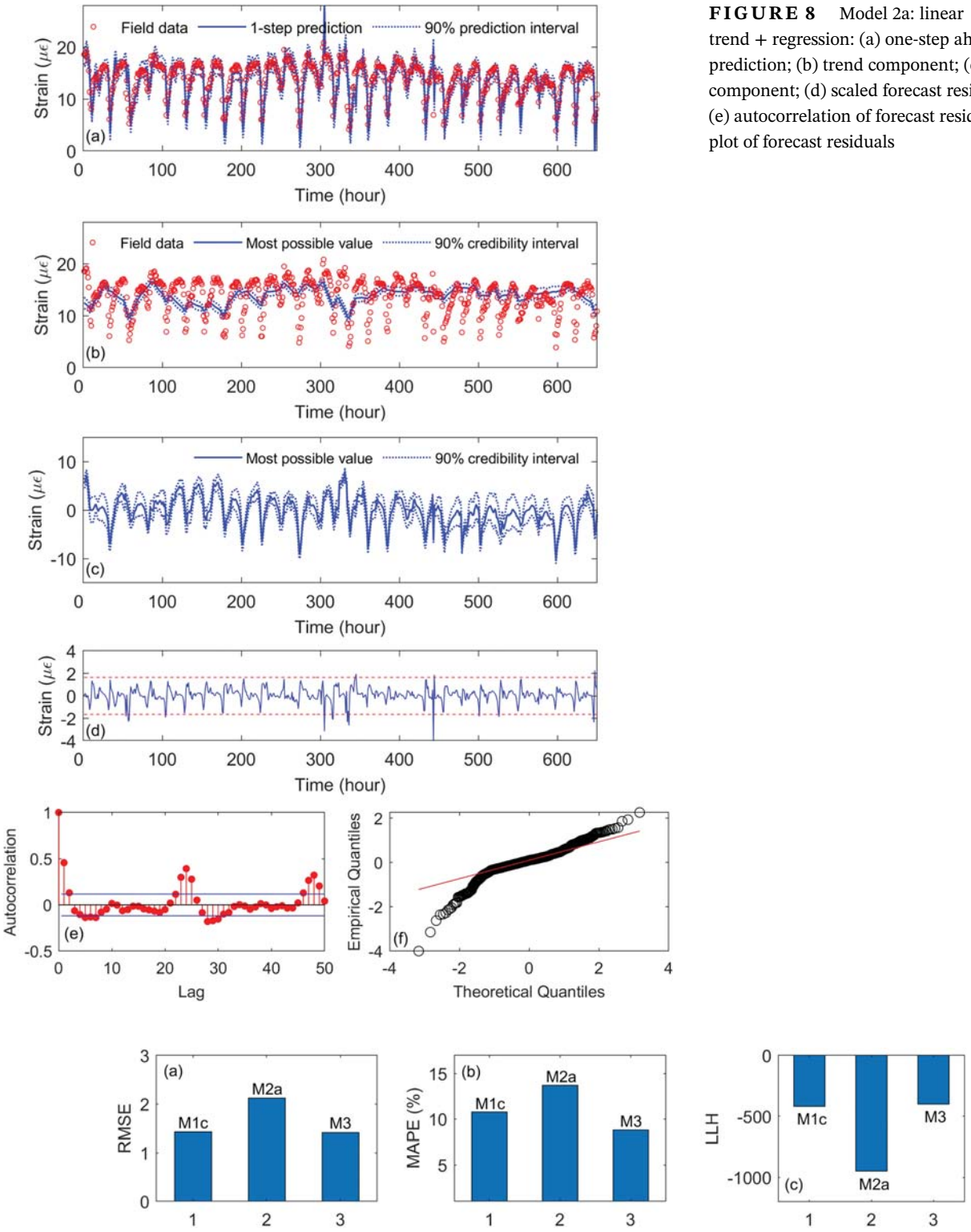

FIGURE 8 Model 2a: linear trend + regression: (a) one-step ahead prediction; (b) trend component; (c) regression component; (d) scaled forecast residuals; (e) autocorrelation of forecast residuals; (f) Q–Q plot of forecast residuals

FIGURE 9 Comparison of forecast performance of model 1c, model 2a and model 3: (a) RMSE; (b) MAPE; (c) LLH

5.2.3 | Model 3: Trend, seasonal (cyclical), and regression

In Model 3, all three components (trend, seasonal [cyclical], and regression) are considered in the DLM for structural strain response,

$$y_t = y_{Tt} + y_{St} + y_{Rt} + v_t, \tag{55}$$

where y_{Tt} is a linear trend, y_{St} consists of three harmonics, and y_{Rt} is a regression component with differential temperature as an explanatory variable.

To obtain a clear picture of the forecast performance, the RMSE, MAPE, and LLH obtained from different models are compared in Figure 9. Obviously, Model 3 with the largest LLH and minimum RMSE and MAPE performs the best, followed by Model 1c and then Model 2a.

The results from Model 3 are plotted in Figure 10. It is seen from Figure 10a that the one-step ahead prediction of strain response is satisfactory on the whole, except for several extreme observations, which lie outside the prediction interval. By comparing the trend component of the three models, it can be found that the trends of Model 3 (Figure 10b) and Model 1c are quite similar and match the underlying trend more closely than that of Model 2a. However, the

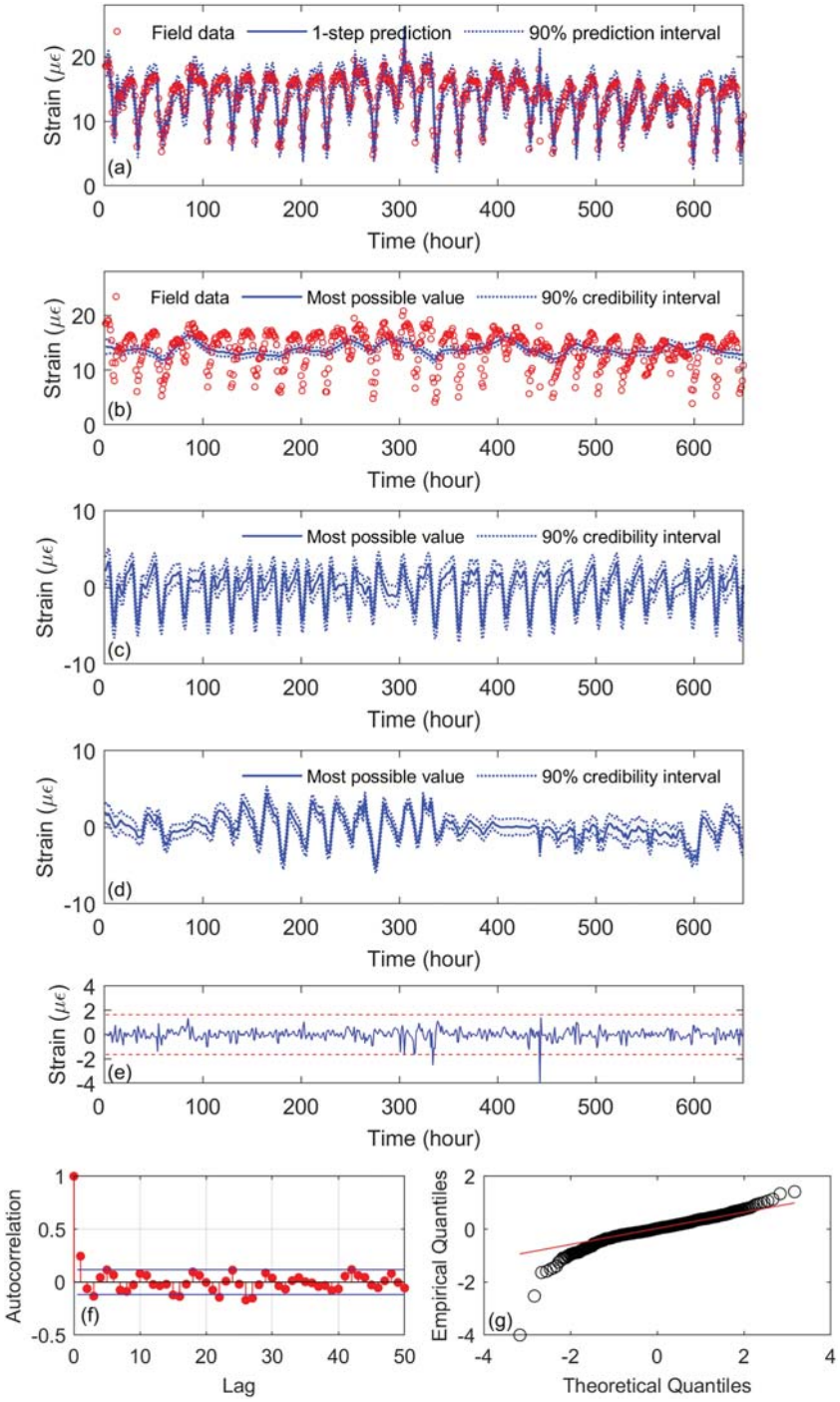

FIGURE 10 Model 3: linear trend + season + regression: (a) one-step ahead prediction; (b) trend component; (c) seasonal (cyclical) component; (d) regression component; (e) scaled forecast residuals; (f) autocorrelation of forecast residuals; (g) Q–Q plot of forecast residuals

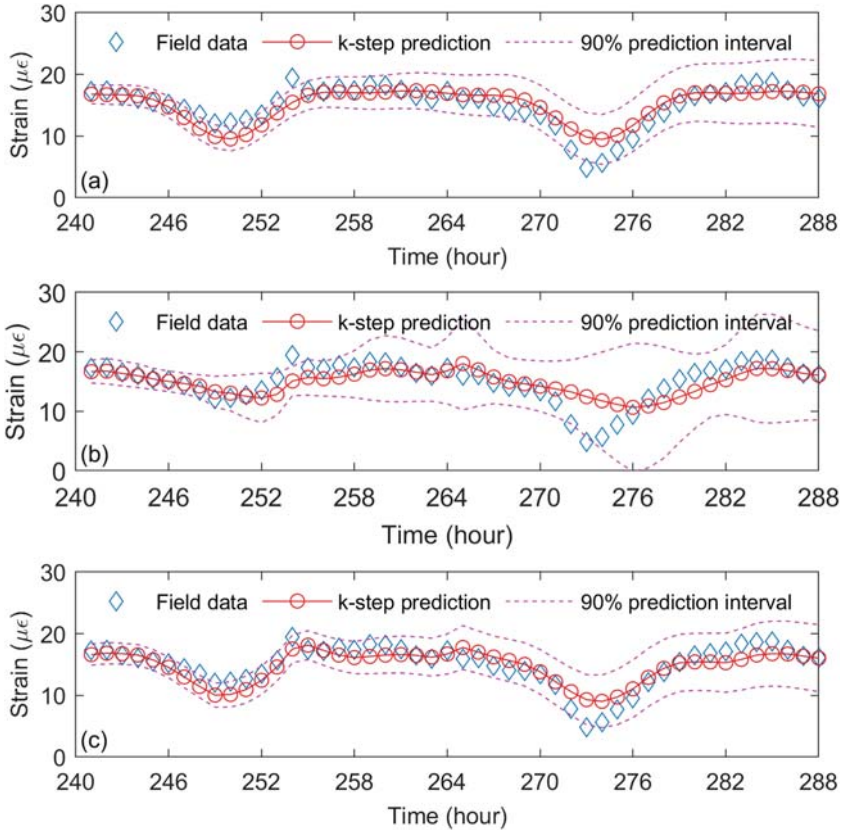

FIGURE 11 *k*-step ahead prediction starting at the 240th hour: (a) model 1c; (b) model 2a; (c) model 3

seasonal (cyclical) effect in Model 3 (Figure 10c) is smaller than that of Model 1c. This phenomenon is due to the fact that the differential temperature effect (Figure 10d) also has seasonal (cyclical) properties and interferes with the seasonal (cyclical) effect. The scaled prediction errors of Model 3 (Figure 10e) are smaller than those of Model 2a and Model 1c, which is further confirmed by the resulting magnitudes of RMSE and MAPE. Similarly, the autocorrelation of forecast errors in Figure 10f is smaller than the preceding models, while the test result of the error normality in Figure 10g is better thanthe preceding models.

5.3 | *k*-step ahead forecasts

In the previous subsection, a thorough investigation on the one-step ahead forecast performance of different models has been made. In this section, also explored is *k*-step ahead forecasting situations in terms of Models 1c, 2a, and 3. Two scenarios are considered: The first scenario is on *k*-step ahead forecasts with starting time at the 240th hour (Hour 240), and the second one is on *k*-step ahead forecasts with starting time at the 500th hour (Hour 500). To

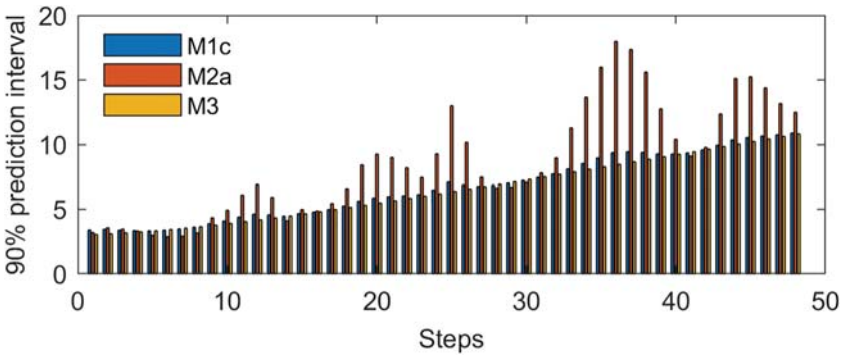

FIGURE 12 Prediction interval of three models

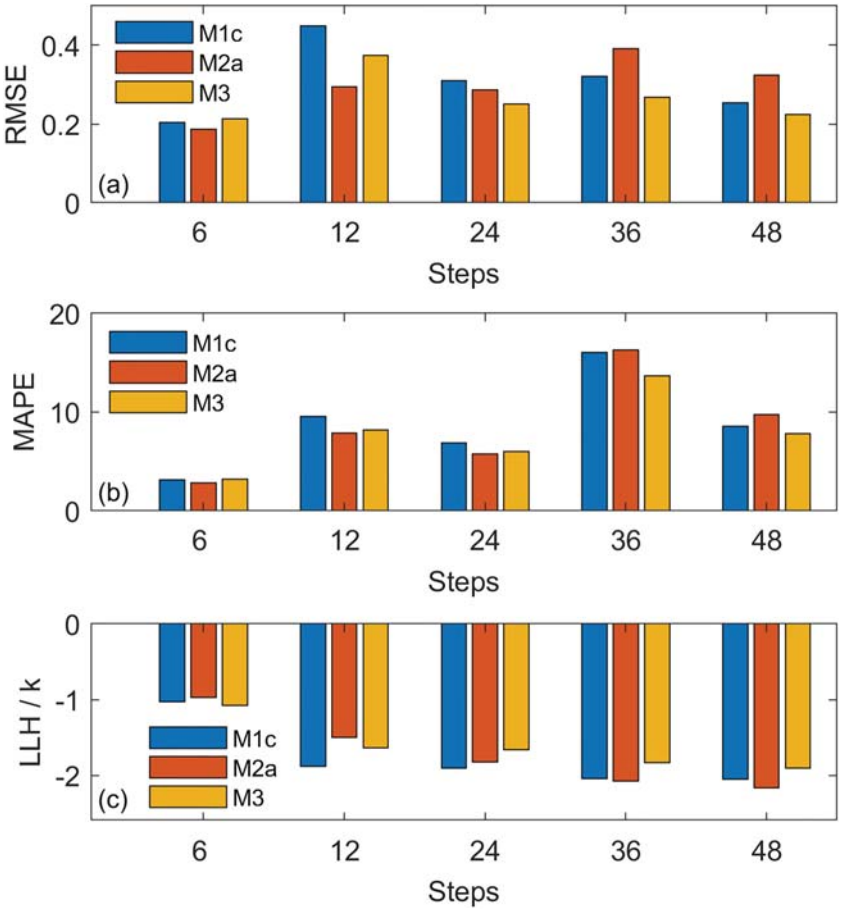

FIGURE 13 Comparison of forecast performance for different models: (a) RMSE; (b) MAPE; (c) LLH/k

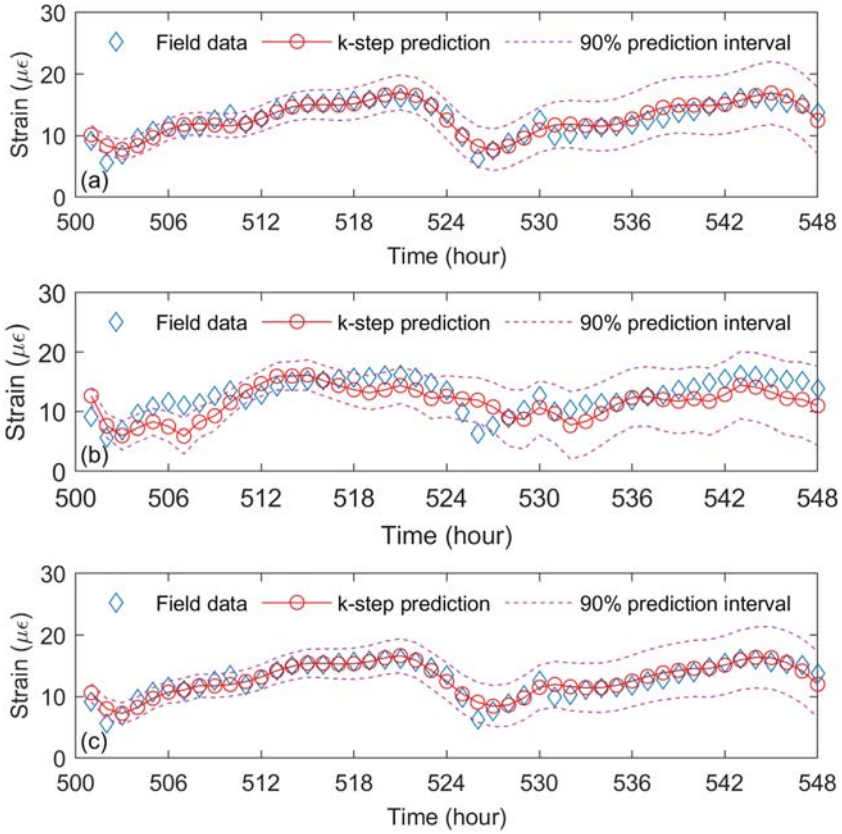

FIGURE 14 *k*-steps ahead prediction starting at the 500th hour: (a) model 1c; (b) model 2a; (c) model 3

compare short- and long-term forecasting performances, a range of different k values, 6, 12, 24, 36, and 48, is tested. As there are 24 observations per day, the above values of k correspond to 6h, 0.5, 1, 1.5, and 2d, respectively.

Figure 11 shows the k-step ahead predictions when the starting time is at Hour 240 for Models 1c, 2a, and 3. Visual inspection makes it evident that the forecast performance of Model 3 is the best, followed by Model 1c and then Model 2a. This is because Model 1c only contains the trend and seasonal (cyclical) components, which changes slowly and cannot make timely adjustments for larger k values, whereas Model 3 with the additional regression component can make adjustments quickly via the differential temperature. The poor prediction performance of Model 2a is due to the lack of the seasonal (cyclical) component, which is vital for characterizing the periodic feature, albeit the regression component also reflects periodicity. For all the three models, most of the observations lie within the 90% prediction interval. Figure 12 shows the comparison of prediction interval (the uncertainty of prediction) for the three models at different prediction steps. It is clear that the prediction interval becomes larger as the number of forecast steps increases. This trend is easy to understand. The ahead forecasts are out-of-sample predictions, hence the further ahead the forecast, the

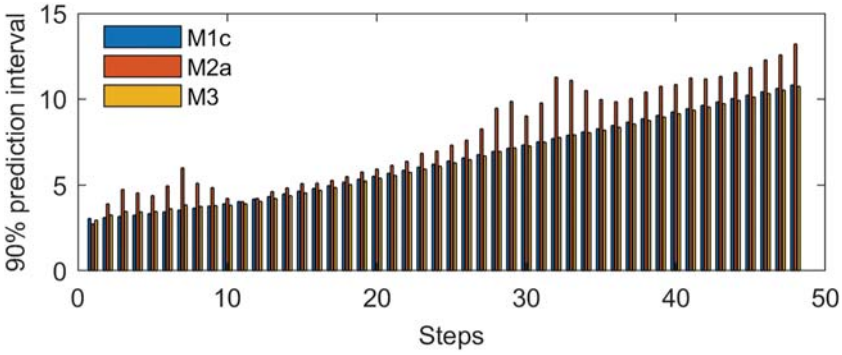

FIGURE 15 Prediction interval of three models

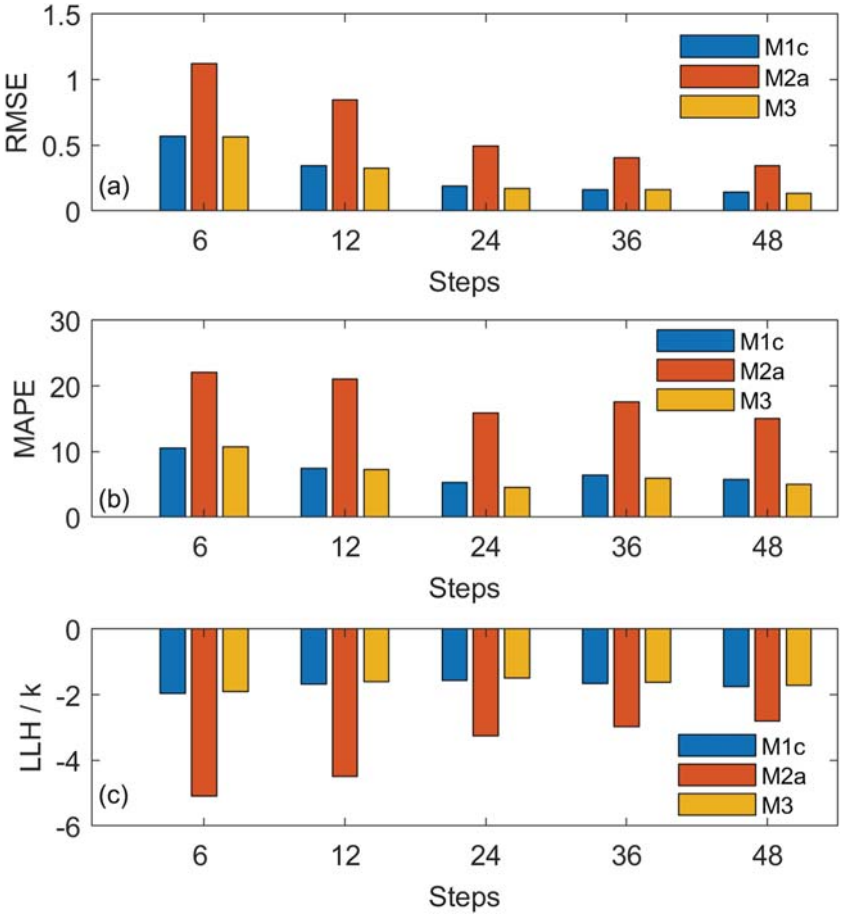

FIGURE 16 Comparison of forecast performance related to different models: (a) RMSE; (b) MAPE; (c) LLH/k

larger the error because of the increasing lack of information. A comparison of the RMSE, MAPE, and *LLH*/*k*metrics for different numbers of step ahead forecasts is also illustrated in Figure 13. For convenience, in comparing *LLH* for datasets of different sizes, the average log likelihood per step *LLH*/*k* is used. Again, it can be concluded that Model 3 outperforms Model 1c and Model 2a.

The results of *k*-step ahead predictions, with staring time at Hour 500 for Models 1c, 2a, and 3, are provided in Figures 14–16. Similar to the previous case, Model 3 is superior to Model 1c and Model 2a, not only in terms of 1 step ahead but also in multistep ahead forecasting performance.

6 | CONCLUSIONS

The present study on the proposed Bayesian modeling approach embedding model class selection for forecasting real-time structural strain response reveals that (i) the proposed method accommodates both stationary and non-stationary time series strain data from SHM system; (ii) it is applicable for simultaneous model class selection and probabilistic forecasts of strain response in a real-time manner; and (iii) it enables quantification of the uncertainty in strain response prediction through obtaining the distribution of predictions.

Application to the strain monitoring data acquired from the TKB demonstrates the feasibility of the proposed method. In terms of the three model performance metrics, that is, LLH, RMSE, and MAPE, the following observations are drawn: (i) the DLM taking account of all three components of trend, seasonal (cyclical), and regression concurrently achieves more accurate strain response predictions than the models with fewer components; (ii) the errors and uncertainty of forecast strain response become larger as the prediction horizon (step) increases. Although the proposed method is powerful for structural response forecasting, a crucial issue should be noticed that if the regressors (such as temperature) are not observed (measured) in parallel, the forecasting execution will inevitably be hindered. To overcome this limitation, a DLM for temperature can be first built for future temperature forecasting, which is then fed into the strain response DLM to enable the strain prediction. The formulated BDLM enables to develop more advanced methods for real-time damage detection.

ACKNOWLEDGEMENTS

The work described in this paper was supported by a grant from the Research Grants Council of the Hong Kong Special Administrative Region (SAR), China (Grant No. PolyU 152024/17E) and a grant from the National Natural Science Foundation of China (Grant No. U1934209). The authors would also like to appreciate the funding support by the Innovation and Technology Commission of Hong Kong SAR Government (Grant No. K-BBY1).

ORCID

Y.W. Wang https://orcid.org/0000-0003-2293-4712
Y.Q. Ni https://orcid.org/0000-0003-1527-7777

REFERENCES

1. Brownjohn JM. Structural health monitoring of civil infrastructure. *Phil Trans Royal Soc London A: Math Phys Eng Sci*. 2007;365(1851):589-622.
2. Wong KY. Instrumentation and health monitoring of cable-supported bridges. *Struct Control Health Monit*. 2004;11(2):91-124.
3. Spencer JBF, Ruiz-Sandoval ME, Kurata N. Smart sensing technology: opportunities and challenges. *Struct Control Health Monit*. 2004;11(4):349-368.
4. Ko JM, Ni YQ. Technology developments in structural health monitoring of large-scale bridges. *Eng Struct*. 2005;27(12):1715-1725.
5. Ni YQ, Xia Y, Liao WY, Ko JM. Technology innovation in developing the structural health monitoring system for Guangzhou new TV tower. *Struct Control Health Monit*. 2009;16(1):73-98.
6. Sohn H, Law KH. A Bayesian probabilistic approach for structure damage detection. *Earthquake Eng Struct Dynam*. 1997;26(12):1259-1281.
7. Sohn H, Czarnecki JA, Farrar CR. Structural health monitoring using statistical process control. *J Struct Eng*. 2000;126(11):1356-1363.
8. Beck JL, Au SK. Bayesian updating of structural models and reliability using Markov chain Monte Carlo simulation. *J Eng Mech*. 2002;128(4):380-391.
9. Beck JL, Yuen KV. Model selection using response measurements: Bayesian probabilistic approach. *J Eng Mech*. 2004;130(2):192-203.
10. Lam HF, Katafygiotis LS, Mickleborough NC. Application of a statistical model updating approach on phase I of the IASC-ASCE structural health monitoring benchmark study. *J Eng Mech*. 2004;130(1):34-48.

11. Lynch JP, Loh KJ. A summary review of wireless sensors and sensor networks for structural health monitoring. *Shock Vib Digest*. 2006; 38(2):91-128.
12. Gul M, Catbas FN. Statistical pattern recognition for structural health monitoring using time series modeling: theory and experimental verifications. *Mech Syst Signal Process*. 2009;23(7):2192-2204.
13. Kopsaftopoulos FP, Fassois SD. A functional model based statistical time series method for vibration based damage detection, localization, and magnitude estimation. *Mech Syst Signal Process*. 2013;39(1–2):143-161.
14. Yu J, Rashid MM. A novel dynamic Bayesian network-based networked process monitoring approach for fault detection, propagation identification, and root cause diagnosis. *AIChE J*. 2013;59(7):2348-2365.
15. Ye B, Shu H, Cao M, et al. A Bayesian network method for quantitative evaluation of defects in multilayered structures from eddy current NDT signals. *Math Probl Eng*. 2014;2014(405707):15.
16. Yuen KV, Mu HQ. Real-time system identification: an algorithm for simultaneous model class selection and parametric identification. *Comput Aided Civ Inf Eng*. 2015;30(10):785-801.
17. Codetta-Raiteri D, Portinale L. Dynamic Bayesian networks for fault detection, identification, and recovery in autonomous spacecraft. *IEEE Trans Syst Man Cybern: Syst*. 2015;45(1):13-24.
18. DeWolf JT, Lauzon RG, Culmo MP. Monitoring bridge performance. *Struct Health Monit*. 2002;1(2):129-138.
19. Wan HP, Ni YQ. Bayesian modeling approach for forecast of structural stress response using structural health monitoring data. *J Struct Eng*. 2018;144(9):04018130.–12.
20. Prakash G, Sadhu A, Narasimhan S, Brehe JM. Initial service life data towards structural health monitoring of a concrete arch dam. *Struct Control Health Monit*. 2018;25(1):e2036.
21. Mei L, Mita A, Zhou J. An improved substructural damage detection approach of shear structure based on ARMAX model residual. *Struct Control Health Monit*. 2016;23(2):218-236.
22. Farahani RV, Penumadu D. Full-scale bridge damage identification using time series analysis of a dense array of geophones excited by drop weight. *Struct Control Health Monit*. 2016;23(7):982-997.
23. Sajedi SO, Liang X. A data-driven framework for near real-time and robust damage diagnosis of building structures. *Struct Control Health Monit*. 2019;27:e2488.
24. Lakshmi K, Rao ARM, Gopalakrishnan N. Singular spectrum analysis combined with ARMAX model for structural damage detection. *Struct Control Health Monit*. 2017;24(9):e1960.
25. Yang N, Bai X. Forecasting structural strains from long-term monitoring data of a traditional Tibetan building. *Struct Control Health Monit*. 2019;26(1):e2300.
26. West M, Harrison J. *Bayesian Forecasting and Dynamic Models*. New York, USA: Springer-Verlag; 1997.
27. Bayesian KG. *Econometric Methods*. New York, USA: John Wiley & Sons; 2003.
28. Solhjell IK. Bayesian forecasting and dynamic models applied to strain data from the Göta River Bridge. M.Sc.Thesis, University of Oslo, Norway. 2009.
29. Goulet JA. Bayesian dynamic linear models for structural health monitoring. *Struct Control Health Monit*. 2017;24(12):1-18.
30. Goulet JA, Koo K. Empirical validation of Bayesian dynamic linear models in the context of structural health monitoring. *J Bridge Eng*. 2017;23(2):05017017.
31. Wang YW, Ni YQ, Wang X. Real-time defect detection of high-speed train wheels by using Bayesian forecasting and dynamic model. *Mech Syst Signal Process*. 2020;139:106654.
32. Lam HF, Yuen KV, Beck JL. Structural health monitoring via measured Ritz vectors utilizing artificial neural networks. *Comput Aided Civ Inf Eng*. 2006;21(4):232-241.
33. Ching J, Chen YC. Transitional Markov chain Monte Carlo method for Bayesian model updating, model class selection, and model averaging. *J Eng Mech*. 2007;133(7):816-832.
34. Cheung SH, Beck JL. Calculation of posterior probabilities for Bayesian model class assessment and averaging from posterior samples based on dynamic system data. *Comput Aided Civ Inf Eng*. 2010;25(5):304-321.
35. Yuen KV, Liang PF, Kuok SC. Online estimation of noise parameters for Kalman filter. *Struct Eng Mech*. 2013;47(3):361-381.
36. Yuen KV, Kuok SC. Online updating and uncertainty quantification using nonstationary output-only measurement. *Mech Syst Signal Process*. 2016;66:62-77.
37. Laine M, Latva-Pukkila N, Kyrölä E. Analysing time-varying trends in stratospheric ozone time series using the state space approach. *Atmos Chem Phys*. 2014;14(18):9707-9725.
38. Roberts GO, Smith AF. Simple conditions for the convergence of the Gibbs sampler and Metropolis-Hastings algorithms. *Stoch Process Appl*. 1994;49(2):207-216.
39. Yuen KV. *Bayesian Methods for Structural Dynamics and Civil Engineering*. New York, USA: John Wiley & Sons; 2010.
40. Ni YQ, Wang YW, Zhang C. A Bayesian approach for condition assessment and damage alarm of bridge expansion joints using long-term structural health monitoring data. *Eng Struct*. 2020;212:110520.
41. Hoff PD. *A First Course in Bayesian Statistical Methods*. New York, USA: Springer; 2009.
42. Petris G, Petrone S, Campagnoli P. *Dynamic Linear Models with R*. New York, USA: Springer; 2009.
43. Kim CJ, Nelson CR. *State-space Models with Regime-Switching: Classical and Gibbs-Sampling Approach with Applications*. MA, USA: MIT Press; 1999.
44. Chib S. Marginal likelihood from the Gibbs output. *J Am Stat Assoc*. 1995;90(432):1313-1321.

45. Ko JM, Ni YQ, Zhou HF, Wang JY, Zhou XT. Investigation concerning structural health monitoring of an instrumented cable-stayed bridge. *Struct Infrastruct Eng*. 2009;5(6):497-513.
46. Ni YQ, Wong KY, Xia Y. Health checks through landmark bridges to sky-high structures. *Adv Struct Eng*. 2011;14(1):103-119.
47. Wang J, Liu X. Evaluation and Bayesian dynamic prediction of deterioration of structural performance. *Struct Infrastruct Eng*. 2010;6(6):663-674.
48. Ni YQ, Hua XG, Wong KY, Ko JM. Assessment of bridge expansion joints using long-term displacement and temperature measurement. *J Perform Construct Facil*. 2007;21(2):143-151.

How to cite this article: Wang YW, Ni YQ. Bayesian dynamic forecasting of structural strain response using structural health monitoring data. *Struct Control Health Monit*. 2020;27:e2575. https://doi.org/10.1002/stc.2575